RE-ENTRY TRACKING FOR APOLLO

BY

F. O. VONBUN

MARCH 6, 1964

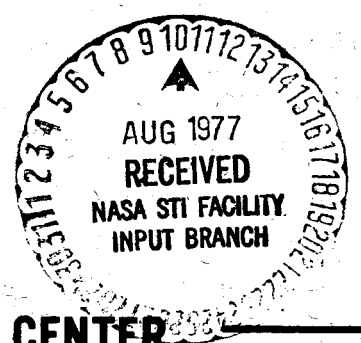

GODDARD SPACE FLIGHT CENTER

GREENBELT, MARYLAND

Md.

RE-ENTRY TRACKING FOR APOLLO

BY

F. O. VONBUN

MARCH 6, 1964

GODDARD SPACE FLIGHT CENTER
GREENBELT, MD.

CONTENTS

SUMMARY

An outline of the re-entry tracking and communication problem including a possible solution is presented in this paper.

The acquisition of the lifting Apollo spacecraft after it enters the earth's atmosphere is a difficult problem for tracking which requires particular attention. An interferometer especially developed for this purpose is described and the major design parameters are given.

A re-entry network configuration is presented, and the necessary tracking tasks outlined. Blackout problems, re-entry trajectory ground tracking errors, the best ship positioning and Goddard's plans to solve the re-entry tracking and communication problems are discussed in detail.

INTRODUCTION

The purpose of this report is twofold, namely

a. To analyze ground tracking and communications problems associated with manned re-entry vehicles, and

b. To develop ways and means to solve these problems in a practical way.

As an entering spacecraft an Apollo-type lifting vehicle is considered, approaching the earth with nearly parabolic speed at a shallow entry angle. A nominal, approximately 5000 nautical mile skip trajectory as presently planned (see ref. 1) is used as an example with a lift to drag ratio of 0.5 and an entry angle of -6.40°.

An effective ground support must be almost independent of the particular trajectory chosen during a real mission. A "nominal" ground track (straight line) as shown in figure 1, 2, and 3 thus cannot be assumed. The ground system must have the capability of covering all possible lifting trajectories the spacecraft is able to fly after it enters the earth atmosphere. The only assumption made here is that the first re-entry point (point #1 in figure 1, 2, 3, 4 and 5) is known to be within ±20 nautical miles (pessimistic value see later) from that previously planned a few hours before actual re-entry into the atmosphere. This is necessary since the re-entry ship could not move fast enough to its proper position in order to assume coverage of the skipout portion as indicated in the figures mentioned. This is not a major restriction since it will be shown later that this point can be determined to well within this error from early return trajectory measurements using in essence the large dish (85') facilities of the Apollo network.

No other restriction shall be considered, so that after the first entry, the spacecraft can fly any trajectory within its capability and the ground system (ship), not knowing the present position of the spacecraft, must acquire it. A hemispherical acquisition capability of the ground tracking system will therefore be considered. It will be shown that an interferometer has this capability, and thus will be used as the spacecraft acquisition system.

Special attention must be given to the blackout areas occurring along the re-entry track due to the transfer of the spacecraft kinetic energy into heat. These areas are of importance for the proper choice of position for the re-entry ship along the track to permit tracking and communication with the spacecraft during the early phase of its skipout as presently planned. An investigation

of the blackout phenomena is under way both in-house and under contract with the University of Alabama, Research Institute. It is anticipated that the outcome of this effort will promote a better understanding and thus better predictions of the blackout areas (see figures 1, 3 and 5), while also giving insight as to methods of combating the blackout problem itself.

Only the "re-entry" phase will be discussed. For purpose of clarification, the re-entry phase is assumed to be that portion of the flight starting with the first build-up of dynamic pressure ($\approx$0.05g, occurring approximately at 400,000 feet for an Apollo-type spacecraft, see figure 1) to the opening of the drag chute ($\approx$90,000 to 70,000 feet), the portion after that is considered as "recovery" and will not be discussed here. Goddard is presently working on a breadboard model of a re-entry interferometer. The system consists of a 1.5 m crossed baseline utilizing five antennas, and will have, an electrical phase error in the order of one degree, an angular error of 0.5 to 5 milliradians over an elevation angle variation from 90° to 10°. Completion of this system is expected in a few months. Airplane tests are then planned using the Goddard calibration aircraft.

I. Apollo Re-Entry Trajectories

In order to have a basis for discussion, a variety of Apollo re-entry trajectories have been chosen as examples in this paper (see references 1, 2, and 3). Typical re-entry trajectories for the Apollo with a $L/D \doteq 0.5$ are shown in figure 1, 2, 3, 4 and 5 with the possible ground tracks which will be of particular concern in this study. Please note that the trajectories shown in these figures (except figure 5) have point #1, the first re-entry point in common and not the landing point which would represent a realistic case. The reason for this is to show that the very first portions of the re-entry trajectories are almost the same in that they are almost independent of the range to be flown. The 5,000 nautical mile trajectory shown in this figure will be considered as a "nominal" re-entry trajectory. It should be emphasized that a "standard" trajectory in the real sense actually does not exist at this time.

The particular re-entry trajectory depends on many variables, such as the entry angle γ (ranging from approximately -4.8° to -6.8°, (see figures 1 and 2), the declination of the moon (see figures 4, 6 and 7 and reference 2 figure 6 and 7)), the inclination of the return trajectory (40° so that under no circumstances can the spacecraft land in the cold regions of the globe, see reference 1). All of this considerably influences the re-entry trajectory and thus the ground track as shown in the figures mentioned. The considerations to be made here although somewhat variable, are applicable to a large variety of re-entry trajectories. This point will be stressed since it is an important one as far as

a proper ground support is concerned. To be effective, a ground tracking network must be nearly independent of the special form of the re-entry trajectory in order to cut down the number of ground stations required. Figure 2 shows a three-dimensional schematic of the re-entry trajectories and the ground tracks for Apollo as depicted in figures 1 and 3. In both graphs the fairly large lateral deviations (hundreds of nautical miles) which the spacecraft is capable of flying are indicated.

From the above it appears almost impossible to intercept the spacecraft with a ground tracker. This fortunately is not so; although the interception or acquisition of the re-entering spacecraft, is the most serious problem which will be discussed later in this paper. A fairly large number of variables influencing the ground tracking system, are known, either from the geometry of the situation or from previous measurements. Examination of figures 4, 5, 6 and 7 helps to answer a few questions.

As an example, lunar departure time, date, and thus the corresponding lunar declination for instance -10° as shown in figures 4, 6 and 7 are accurately known. This together with the down range length of the re-entry trajectory determines to a certain extent the "preferred" landing site. (See reference 2) Also known, from the mission and from tracking information during the last three days of the return flight, is the inclination i_R of the return trajectory phase within the accuracy limits of our present tracking systems and orbital theories used. The entry point #1 (figures 1, 2, 3, 4, 5, and 6) can be determined easily to within a few nautical miles using tracking information from the Apollo tracking network measuring range, range rate and angles.

All of this information can be used for advance planning of the location of the tracking ships and aircraft as necessary for supporting the earth re-entry portion of the lunar return.

II. Problems of Spacecraft Acquisition

One of the most severe ground support problems encountered during the re-entry of the spacecraft, as mentioned, is that of acquisition. This can be seen by examining figures 1, 2, 3 and 8. The maximum lateral deviations of the trajectories, as indicated in figures 1 and 3, reach a value of $\approx$700 nautical miles at a distance of 5,000 nautical miles from the first re-entry point #1. Figure 3 also shows the circles of visibility of the ship for elevation angles $\epsilon = 10°$ (interferometer acquisition) and $\epsilon = 3°$ (communications). The circles of visibility for a spacecraft height H = 300 kft are left open intentionally on this figure because acquisition can be obtained only when the spacecraft is almost

overhead. (See figure 8 and figure 3 for more details.) It further indicates the probability distribution of the trajectories which will be flown. This curve, contrary to all other data shown in figure 3, is a schematic only and not a calculated one (depends on spacecraft equipment only). It only should demonstrate here that it is more probable that trajectories close to the nominal one will actually be flown, thus making the interferometer circle (ϵ=10°) as shown really adequate for acquisition. All considerations will depend on the first entry point location #1 and adequate knowledge in advance. It can be seen that an unpredicted variation of even 50 nautical miles would not harm the acquisition problem. It will be shown later that under pessimistic tracking assumptions, the orbit can be determined to adequately fix point #1.

In the following, emphasis will be placed on a special interfermetric acquisition system suggested by J. T. Mengel and the author some time ago. (See reference 4 page 13.) It is assumed that the USBS* beacon onboard the spacecraft is radiating a cw-signal, that the spacecraft antennas are in operation, and that the spacecraft is beyond the blackout areas shown in figure 1, 3 and 5.

Note that even when all the conditions mentioned are met, it may still be impossible to contact the spacecraft by radio. This can be seen from figure 6, which shows the spacecraft antenna pattern for positive lift position. As shown here radio contact would be obtained only for the period of time when the spacecraft is almost above the tracking station and thereafter.

A "spill-over", usually not wanted from antennas in general, would be highly desirable for this special case of the Apollo omni-antennas. Also, considerations are given to the use of IR and skin tracking radar scanning techniques in case the spacecraft transmitter is not operating or the craft is still within the radio blackout regions. (See figures 1, 3 and 5.)

The problem of acquisition is the same in both cases since it stems from the fact that the lifting spacecraft can deviate a considerable lateral distance from the nominal track as shown in figure 1, 2 and 3.

In order to be able to cover all flight possibilities it is assumed that "no a priori" information is available when and where the spacecraft reaches the exit point A, A′ shown in figure 1 and 3. This, of course, constitutes the most undesirable case. It is felt, however, that a proper ground network has to cover the region of spacecraft flight capability given by γ, L/D and entry velocity v as depicted in figure 1, 2 and 3. Based on this, a search capability for

*USBS stands for Unified S-Band System. This system combines tracking (range and range rate, JPL's pseudo random code) and communications thus forming a single system for both tasks.

the entire hemisphere has to be built into the tracking acquisition system. This is true for both cases, the cooperative as well as the non-cooperative systems for acquisition. An additional requirement which has to be met by these systems is that of short acquisition time. Short time here means a time in the order of one to two seconds.

Assuming a spacecraft height of approximately 70 km (≈200kft) (see figures 2 and 5) and a speed in the order of 7 to 7.5 km/s during the first portion of the re-entry maneuver a maximum angular rate (ϵ near or equal to 90°),

$$\dot{\epsilon} \doteq \frac{v}{h} \doteq \frac{1}{10} \text{ rad/s} \doteq 6^{o/s} \tag{1}$$

is to be expected. As mentioned earlier, not knowing the position of the spacecraft and its possible great angular speed, if over head (see figure 8) creates real problems for spacecraft acquisition.

These are the reasons why special acquisition systems are being developed for an Apollo-type re-entry.

III. Special Re-Entry Acquisition Systems

Taking into account the existing acquisition problems after re-entry (see point #2 in figure 1 and 5) led to the concept using an interferometer with fixed, broad beam antennas as an acquisition aid. The advantage of such an instrument, proved in over six years of operation of the Minitrack system, is that no moving antennas such as in the case of search radars, and nearly hemispherical coverage (10° above horizon) can be obtained as indicated in figure 9).

Assuming that the spacecraft USBS transmitter radiates a cw-signal the omnidirectional individual interferometer antennas can receive this signal from which the phase difference ϕ can be determined using phase measuring techniques (see reference 5, 6, 7, 8, 9 and 10 for more details). From this phase

$$\phi = 2\pi \frac{s}{\lambda} \tag{2}$$

the angle α_1 as shown in figure 9 can be determined by:

$$\cos \alpha_1 = \frac{s}{b} = \frac{\phi\lambda}{2\pi b} \tag{3}$$

knowing the wavelength λ, the antenna separation b and the phase difference ϕ (measured). The angles α_1 between the position vector of the spacecraft $\vec{r}$ and the NS- baseline and α_2, the equivalent in the EW direction, determine the local unit position vector $\vec{r}^{\circ}$ of the spacecraft.

This determination of $\vec{r}^{\circ}$ solves the acquisition since a small dish then can be directed, with this knowledge, toward the spacecraft to accomplish a range measurement r and also to establish communications.

The local spacecraft position vector $\vec{r}$ is then given by

$$\vec{r} = r \cdot \vec{r}^{\circ} \tag{4}$$

and this spacecraft position vector can be used to check the spacecraft re-entry trajectory $\vec{r} = f(t)$.

Before continuing it may be appropriate to derive some of the major design parameters for such a re-entry interferometer. Varying equation (3) with respect to ϕ, λ, and b, and collecting terms results in

$$\delta\alpha_1 = \frac{1}{2\pi \sin \alpha_1}\left(\frac{\lambda}{b}\right)\left[\delta\phi + 2\pi\left(\frac{b}{\lambda}\right)\cos\alpha\left(\frac{\delta\lambda}{\lambda} - \frac{\delta b}{b}\right)\right] \tag{5}$$

The frequency (wavelength) can be considered as constant during the time the wave reaches the two interferometer antennas, that is $\delta\lambda=0$; one then obtains from equation (5) the following error in α_1 using the Gaussian principle of propagation of errors.

$$\sigma_\alpha = \frac{1}{2\pi \sin\alpha}\sqrt{\left(\frac{\lambda}{b}\sigma_\phi\right)^2 + \left(2\pi\cos\alpha\,\frac{\sigma_b}{b}\right)^2} \tag{6}$$

Utilizing a proper "balance" between the obtainable errors σ_ϕ in the electrical phase measurement and σ_b the error in the baseline length one obtains for σ_α the following values with 1 (see reference 5 for more details)

$$\lambda = 15\,\text{cm},\ b = 1.5\text{m},\ \frac{\lambda}{b} = \frac{1}{10}$$

$$\sigma_\phi = \frac{1}{57}\ \text{rad}\,(\sim 1°),\ \sigma_b = 0.1\,\text{cm}$$

$$\text{for } \alpha = 90°\ldots\ \sigma_\alpha = 0.5\ \text{mrad};\ \alpha = 10°\ldots\ \sigma_\alpha = 5\,\text{mrad}.$$

Figure 10 shows the expected angular error σ_α in mrad as a function of the angle α for an assumed electrical phase measuring error of 1° and baseline length errors of 1, 2 and 3 mm as indicated on the graph. These angular errors will later be used to estimate the errors of the skipout trajectory and thus those of the second re-entry point (point #3 in figure 1, 5 and 11).

An interferometer (breadboard model) of this kind designed especially for re-entry acquisition of the Apollo spacecraft is presently under construction at Goddard. It is planned that the ground plane accommodating both perpendicular base lines (see figure 9) as well as all the ambiguity antennas will measure less than approximately 10' x 10'.

The output of this interferometer will be the equivalent to angles α_1 and α_2 as shown in figure 9 (that is the unit position vector $\vec{r}°$ from the ground station to the spacecraft) as well as their rates $\dot{\alpha}_1$ and $\dot{\alpha}_2$ (or $\dot{\vec{r}}°$).

IV. Tracking Station Locations Along the Re-Entry Ground Track

In the following will be shown the optimum position for a ground tracking station (ship) in order to support the entering lunar spacecraft. Position here means the location of the tracker on earth in respect to the lifting re-entry trajectory. Figure 12 shows the position of the re-entry ship and of the aircraft necessary to support the re-entering spacecraft with communication capability. Since the same aircraft are being used that were used for injection (that is communications coverage during the S-IV-B burn out of the parking orbit into the lunar transfer orbit, a mandatory requirement) they are thus available. They are depicted only in figure 12 to show that 5 aircraft together with the necessary re-entry ship can cover the total 5,000 nautical mile re-entry track. Removing aircraft A_2 or A_3 will still cover most of the trajectory

which may be enough if only a total of four aircraft are available. This is strictly dependent on the mission requirement which is beyond the scope of this paper.

Before continuing into re-entry tracking, several facts should be taken into account, facts already known as well as facts predicted or calculated based on measurements made during the time on the earth return flight which will last approximately 70 h as presently planned.

The lunar take-off time, and thus the declination of the moon δ m, the planned inclination i_R of the return trajectory (see figure 4) and the time characteristic are known. From these data the earth landing site can and will actually be chosen as shown in figure 6 and 7 (see also references 1 and 2). These figures show the areas of first re-entry (point #1) for northern and southern landings. It should be noted that the landing points finally chosen will not alter the considerations here to a great extent since the coverage which has to be provided by the re-entry network using ships and aircraft is fairly independent of the particular landing point chosen for the real mission. Tracking information collected during the relatively long ($\approx$70 h) return flight will be used to alter the return trajectory by using proper midcourse maneuvers to assure that the first re-entry point coincides with that previously planned. Figure 13 depicts a possible return trajectory for landing in the Hawaiian area. This trajectory is used as an example to show that tracking information using only the Canberra 85' dish and the Indian Ocean ship's* 30' dish is adequate for our impact point #1 determination. To be real pessimistic, it is assumed here that tracking information only from a distance of 51,000 nautical miles, that is 8h before entry, is available for orbit determination. The reason here is not to show how well the orbit can really be determined but rather to demonstrate that tracking with one 85' dish when the spacecraft is still a few hours out and one 12' or a 30' dish on the Indian Ocean ship is adequate from a ground tracking point of view to locate the re-entry ship in advance (see figure 12). Even without this ship the entry point #1 would be known well enough for this purpose. It should be emphasized that these loose requirements here are only related to the re-entry ships location and acquisition problem and not to the tighter requirements from the aerodynamic re-entry point of view. The re-entry angle for instance is a critical parameter as far as atmospheric re-entry is concerned as outlined in references 11, 12 and 13. Figure 14 shows the errors associated with the entry under these loose conditions stated above. A tracking sampling rate of one range, range rate, azimuth and elevation measurement per minute is assumed.

*Please note that this ship is located at approximately 60 °E and 25 °S to cover the post injection phase (7 min. coverage) and can be moved during the seven days of the mission to a location of approximately 90 °E and 10 °S to cover the approaching spacecraft for minutes (6 to 7 min.) before it reaches the atmosphere at 400 kft.

Figure 6 (extracted from reference 2) shows the locus of the re-entry points (designated as #1 in figure 1, 2, 3, 4, 5, 6 and 7) for an Hawaiian water landing. The limitations given are only those of the lunar declinations δ_m, the maximum re-entry range of 5000 nautical miles and the maximum inclination of the lunar return trajectory $i_R \doteq 40°$. The reason for this was operational in order to assure that under no circumstances or possible failures can the spacecraft land in the cold regions of the earth assumed to be above or below 40° latitude. Figure 7 shows a similar graph for a southern landing.

Figure 12, an extract of figures 4 and 6, shows in more detail the possible re-entry trajectory for a chosen example, namely $\delta_m = -10°$ and a return inclination $i_R = 20.2°$.

In this case, it can be seen that only the $i_R = 20.2°$ return trajectory would be 5,000 nautical miles long assuming the landing point is given using different return inclinations.* Using this example the tracking ship would have to be placed approximately 1,000 nautical miles down range from point #1 as indicated in the previous graphs.

The odd shaped areas of coverage for tracking (elevation angle $\epsilon = 10°$ for the interferometer on the ship (dark area) and communications ($\epsilon = 5°$, aircraft height $\doteq$ 30,000 ft.) are due to the height variation of the spacecraft flying the re-entry trajectory as shown in figure 1. Comparison of the dark area representing the tracking capability of the ships acquisition interferometer ($\epsilon = 10°$), and the maximum deviation of the spacecraft depicted in figures 1 and 3, show that acquisition should be possible under any circumstances. Again, it should be pointed out that the "final" position of the ship will depend on the real blackout areas (which by this time will hopefully be better determined than at the present time) and the real lateral flight capability of the spacecraft. Figure 3 gives a better view of the beginning of the re-entry phase. As shown here, the ship is placed just "outside" of the blackout area approximately 1,000 nautical miles downrange from point #1.

Blackout areas are considered to be those areas along the re-entry trajectory where the electron density is so high that communication between the re-entering spacecraft and a ground station is impossible. The frequency regions considered for this definition are those commonly used for communications up to 10 kmc. (See reference 14 for more details.) The reason for the

*The following simplifying assumptions have been made (see reference 2, p-2): constant earth moon distance; a constant vacuum perigee; a constant true anomoly of 174°; only the earth's gravitational field acting on the vehicle.

increased electron density in the vicinity of the entering spacecraft is the transfer of the kinetic energy of the spacecraft (braking action of the upper region of the earth's atmosphere) into heat, predominently by compression in the stagnation region but partially by skin friction in the boundary layers. Figures 1, 3 and 5 show these areas of radio blackout from Apollo-type vehicles as they are known at this time (see reference 14). As can be seen from figure 5, considerable differences exist (up to $\approx$400 nautical miles in distance) in the duration of these regions, indicating that more studies are required to clearly define them. As indicated in the graph, up to 50% of the total communications time could get "lost" due to an extension of the blackout region. After this brief consideration of the radio blackout problem, which is important as shown for positioning the re-entry ship, let us go back to the tracking ship and its acquisition problems. Also indicated on figure 3 is the ship's initial acquisition angle $\alpha_{s_{in}} \doteq 75°$ for this case. Immediate acquisition is difficult to get due to the antenna pattern and the attitude of the spacecraft. As shown in figure 8, antenna "spillover" may be enough to make acquisition possible. This in turn suggests the desirability of not using too "good" a spacecraft antenna design. The spacecraft could emerge within an angle of 75° at minimum, taking the worst condition when the spacecraft flies a short and one-sided trajectory (maximum deviations of the ground track end-points). In case acquisition cannot be obtained right away, the angle $\alpha_{s_{in}}$ could increase to almost 180° (not quite since the interferometer minimum elevation angle is approximately 10°). By placing the ship in the indicated position, it is assured that the "ship visibility" exceeds the maximum lateral maneuverability of the spacecraft as indicated in figure 3.

Assume now that the spacecraft has been acquired at a point X and is tracked over a time period of time T during its "free flight" skipout as shown in figure 11 (compare also with figure 1). The question then arises as to what errors η_{pos}, η_{vel}, can the position and velocity of the craft be determined approximately at the point C when it leaves the visibility region of the ship and what is the magnitude of these errors η^*_{pos}, η^*_{vel} transformed to the second re-entry point (#3)? Figures 15 and 16 give the answer to these questions using an interferometer as described before on the ship for acquisition and angular information α_1, α_2 as well as a small dish for range and range rate information (USBS) with and without ship location errors.

An error in the location of the ship of ±1 km in latitude and longitude has been assumed for the calculations depicted in figure 16 (see reference 15, 16 and 17). Figure 15 and 16 shows both the position and velocity errors at the end of the tracking as well as the projection of these errors to the second re-entry. As indicated for short tracking times in the order of seconds, that means acquisition has been accomplished relatively late, (acquisition point X is near C in figure 11) the errors are relatively large and so are their projections to

point #3. Nevertheless all are within the limits of the spacecraft dynamic flight capability. Assuming that acquisition is accomplished late (to be on the pessimistic side) so that only a short time $T \doteq 40$ seconds remain for tracking the errors are $\eta_{pos} = 1360$m, $\eta_{vel} = 11$m/s and their projections are $\eta^*_{pos} = 34{,}000$m, $\eta^*_{vel} = 15$m/s as seen from figure 16. Under the assumption that the errors in the location of the ship are ±1000 m (3,300 feet) in longitude and latitude respectively. It is felt at this time that it is appropriate to give an additional description of the prepositioning of the re-entry tracking ship as shown in figure 1, 3 and 12.

Since the ship is prepositioned during the last few hours of the mission due to its slow velocity and can be considered a fixed station, certain precautions for the proper re-entry coverage have to be taken. Fortunately these, as will be shown are very relaxed ones which means that the ground net, in this case the prepositioned re-entry tracking ship, imposes no limitations on the mission.

To make sure that the ship can "see" the spacecraft even with possible variations due to "last minute" maneuvers of the spacecraft, changes of the entry point #1 are considered next.

These variations along and perpendicular to the re-entry track can be expressed in a simple form by:

$$\delta_{perp} \doteq \frac{(R + h)}{v_o \cos \gamma_o} \cdot \delta v_{o_{perp}}$$

$$\delta_{track} \doteq \frac{(R + h)}{\gamma_1} \sqrt{\frac{2r_o}{\mu}} \, \delta v_{o_{track}} \tag{8}$$

where R is the earth radius, h is the height of the re-entry point above earth, γ_o is the flight path angle for r_o and v_o, v_o the velocity where a velocity maneuver of $\delta v_{o_{perp}}$ or $\delta v_{o_{track}}$ is to be executed at a distance r_o from the center of the earth, μ is the gravitational parameter and γ_1 is the re-entry flight path angle (-5° to -7°). Equations (8) are based on simple Keplerian orbits using the earth as the only attracting body. Varying these orbital equations with respect to the velocity and neglecting higher orders terms result in the equations (8) stated above, giving the variations perpendicular and along the re-entry track. Figures 17 and 18 present equations (8) in graphical form. As can be seen "wrong maneuvers" in the perpendicular direction up to $\delta v_{o_{perp}} \doteq 9$ ft/s as much as 4-1/2h or $r_o = 32{,}500$ nmi out would not make it

necessary to alter the ship's position. From figure 18 it can be deducted that a "wrong" change in velocity along the tangent $\delta v_{o\,tang} \doteq 9$ ft/s performed 4-1/2 h out would result in a change $\delta_{track} \doteq 60$ nautical miles for the re-entry point #1, which also is not dangerous from the ground tracking point of view since it would only result in a tracking time loss of approximately 10 seconds. Not "recorded" variations $\delta v_{o\,track} \doteq 30$ ft/s as much as 10 h out ($r_o \doteq 64{,}000$ nautical miles) would on the other hand, reduce the tracking ship's usefulness since the change of $\delta_{track} \doteq 270$ nautical miles would bring the blackout region beyond the tracking ship as shown in figures 1 and 3. But even under these conditions, not too much harm would be done. This shows that the prepositioning of the ship is indeed possible.

Figures 17 and 18, on the other hand, show also what changes of point #1 on the earth can be accomplished when the tracking data and thus the nominal return trajectory indicates that the entry point #1 is not where previously planned in order to optimize the ground tracking capability if found necessary.

V. Goddard's Effort to Solve the Re-Entry Tracking and Communications Problem

As mentioned in the course of this paper, Goddard is presently building a breadboard model of a re-entry interferometer (acquisition system for the USBS) hopefully to be used finally for the Apollo entry acquisition and tracking. The ground plans dimension will be approximately 10' x 10'. Four racks of electronic equipment will, with a display console, constitute the total system. It is anticipated that this breadboard model will be in operation by July 1964. At this time it is planned to perform aircraft tests using one of Goddard's calibration airplanes (DC-6). A USB-transponder and proper antennas will be installed in the aircraft to simulate acquisition and study the problems in more detail.

Studies are also under way at Goddard (references 18 and 19) to investigate the possibility of utilizing the generated re-entry heat (infrared) to acquire the spacecraft. This is of importance particularly for aircraft in order to direct the USB antennas toward the entering spacecraft to establish communications. Also here hemispherical search capability is of importance in order to cover all possible re-entry flights during the spacecraft's early dynamic and ballistic (skip) paths.

As mentioned also, radio blackout, particularly its beginning and ending period during certain portions of the re-entry flight constitute a problem. In order to gain more insight in this area, Goddard has negotiated two contracts.

One with Dr. F. J. Tischer, Associate Director, Research Institute, University of Alabama, Huntsville, Alabama, who will continue the theoretical investigations he started some time ago as member of the staff of the Systems Analysis Office at Goddard. The expected results of this study will be more sophisticated mathematical models of the ionized flow field and the radio frequency propagation through this flow field during super orbital re-entries into the earth's atmosphere. These models will have to contain semi-empirical terms which at this time cannot be rigorously determined theoretically. In order to obtain in a parallel fashion experimental results, Goddard has negotiated a second contract with Cornell Aeronautical Laboratory, Inc., Buffalo, N. Y. (Mr. Hertzberg). Those experiments, theoretically guided by both institutions and performed in the unique shock-tube wind tunnel facility at Cornell appears to be a most promising approach to attack the blackout phenomena. Actual radio wave propagation measurements will be performed in the well-surveyed flow field surrounding the model under simulated transmitting conditions of the re-entering spacecraft. Experiments to study ablation effects, fluid injection and local magnetic fields surrounding the antenna (control of the tensor characteristic of the plasma) will also be investigated experimentally at Cornell. It is hoped that with this two-pronged approach, real progress can be made toward a solution of the blackout problem acceptable to the final operation during re-entry or this last phase of the lunar mission.

Based on this paper, anticipated comments, and probable changes in the mission rules, a more comprehensive document will be published in the future.

ACKNOWLEDGMENT

The author wishes to acknowledge the assistance of Mr. J. T. Mengel in reviewing this report and Mrs. A. Marlow, Mr. T. Jones, Mr. R. Groves and in particular Mr. W. Kahn in the preparation of it. In addition the author wishes to thank Mr. L. Jenkins, Mr. J. Hodge, Mr. J. Mayer, and Mr. C. Kraft of the Manned Spacecraft Center for their helpful discussions on this subject.

REFERENCES

1. Flight Operations Division, "Trajectory Studies for use in Determining Tracking Requirements for Project Apollo", M.S.C., Mission Planning Department, August 30, 1963.

2. Groves, R. T., "Re-Entry Range Requirements for the Apollo Lunar Mission with Operational and Geometric Constrains", Systems Analysis Office, Working Paper, GSFC, December 13, 1963.

3. Vonbun, F. O., "Re-Entry Concept for Apollo", Systems Analysis Office, Working Paper, GSFC, June 21, 1963.

4. Vonbun, F. O., "Parking Orbits and Tracking for Lunar Transfers," GSFC Report X-520-62-63 Fig. 10, June 7, 1962.

5. Simas, V. R., "A System for Re-entry Tracking of the Apollo Spacecraft," GSFC Rept. X-523-63-56, April 2, 1963.

6. Schoeder, C. A., Looney, C. H., Carpender, H. E., "Tracking Orbits of Man-made Moons," Electronics, January 2, 1959.

7. Mengel, J. T., "Minitrack Systems Design Criteria," Electr. Engr. 76, pp 666-667, 1957.

8. Mengel, J. T., "Tracking the Earth Satellite, and Data Transmission by Radio," Proc. IRE 44(6) 755-760 June 1956.

9. Simmon S, G. T., "A Theoretical Study of Errors in Radio Interferometer type measurements Attributable to Variations in the Medium," IRE Trans. Tel. & Comun. pp 2-5, Dec. 1957.

10. GSFC Rept X-531-63-251, "Phase Measurement/Display Subsystem for the Apollo Re-Entry Tracking System", December 13, 1963.

11. Young, J. W., Russel, W. R., "Fixed-Base Simulator Study of Piloted Entries into the Earth's Atmosphere for a Capsule-Type Vehicle at Parabolic Velocity", NASA TN D-1479, Oct. 1962.

12. Assadourian, A., Cheatham, D. C., "Longitude Range Control During the Atmospheric Phase of a Manned Satellite Re-Entry", NASA TN D-253, 1960.

13. Foudriat, E. C., Wingrove, R. C., "Guidance and Control During Direct-Descent Parabolic Re-Entry", NASA TN D-979, 1961.

14. Lehnert, R. L., Rosenbaum, B., "Plasma Effects on Apollo Re-Entry Communications," GSFC Rept. X-513-64-8, Jan. 1964.

15. Vonbun, F. O., Kahn, W. D., "Tracking Systems, Their Mathematical Models and Their Errors, Part I - Theory, NASA TN D-1471, Oct. 1962.

16. Kahn, W. D., Vonbun, F. O., "Tracking Systems, Their Mathematical Models and Their Errors," Part II - Least Square Treatment, to be published soon as NASA Technical Note.

17. Cooley, C. L., "Tracking Systems, Their Mathematical Models and Their Errors," Part III - Program Description, to be published soon as a GSFC Rept. and NASA Technical Note.

18. Plotkin, H. H., "Infrared Re-Entry Tracking," GSFC Rept. X-524-62-136, Aug. 10, 1962.

19. Minott, P. O., "A Study on the Feasibility of Infrared Re-Entry Acquisition of the Apollo Spacecraft", GSFC Rept. X-524-64-53, to be published soon.

20. GSFC, Tracking and Data Systems Directorate, "A Ground Instrumentation Support Plan for the Near-Earth Phases of the Apollo Mission", GSFC Rept. X-520-62-211, Nov. 23, 1962.

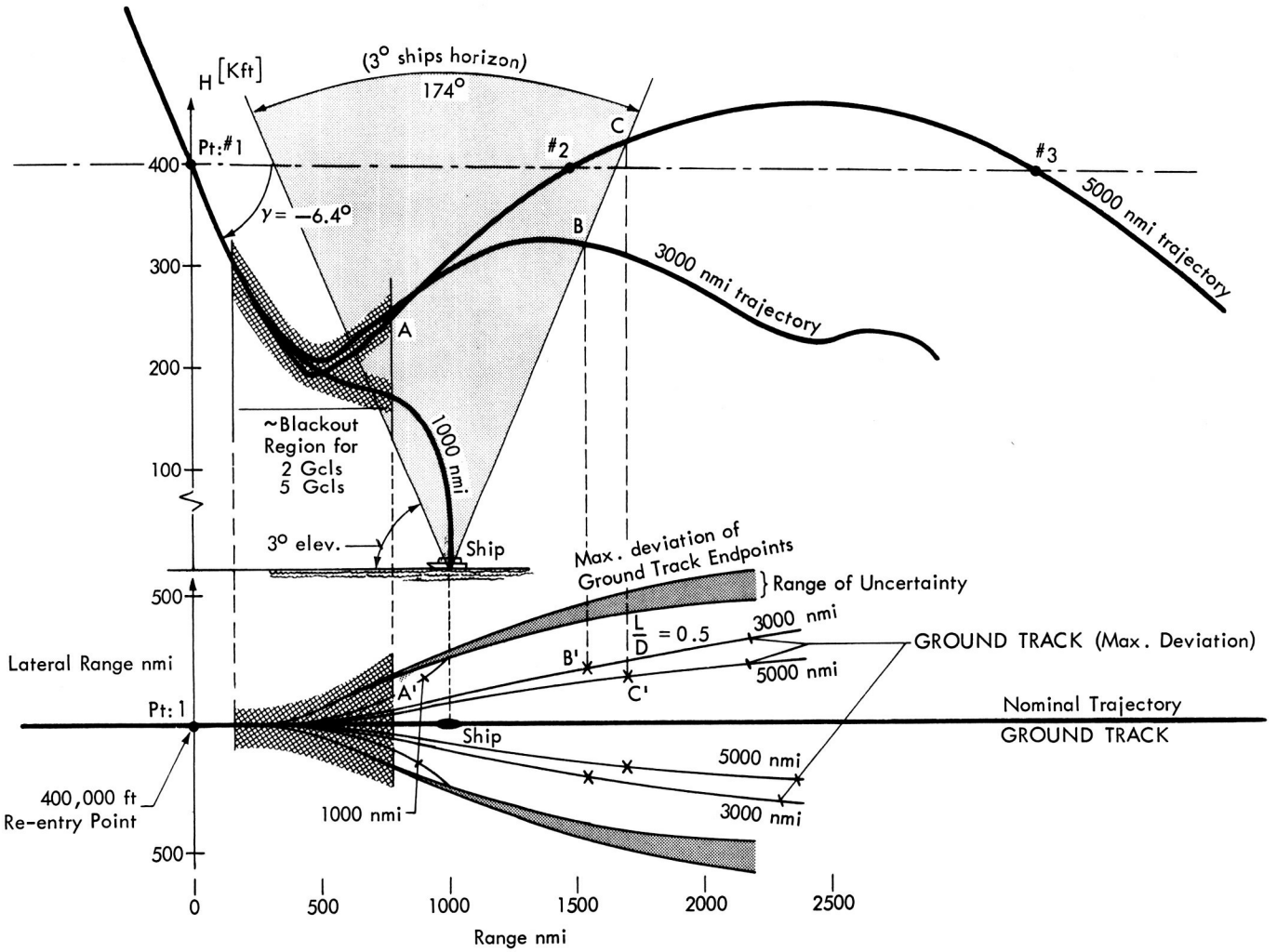

Figure 1 - Apollo Re-Entry Trajectories

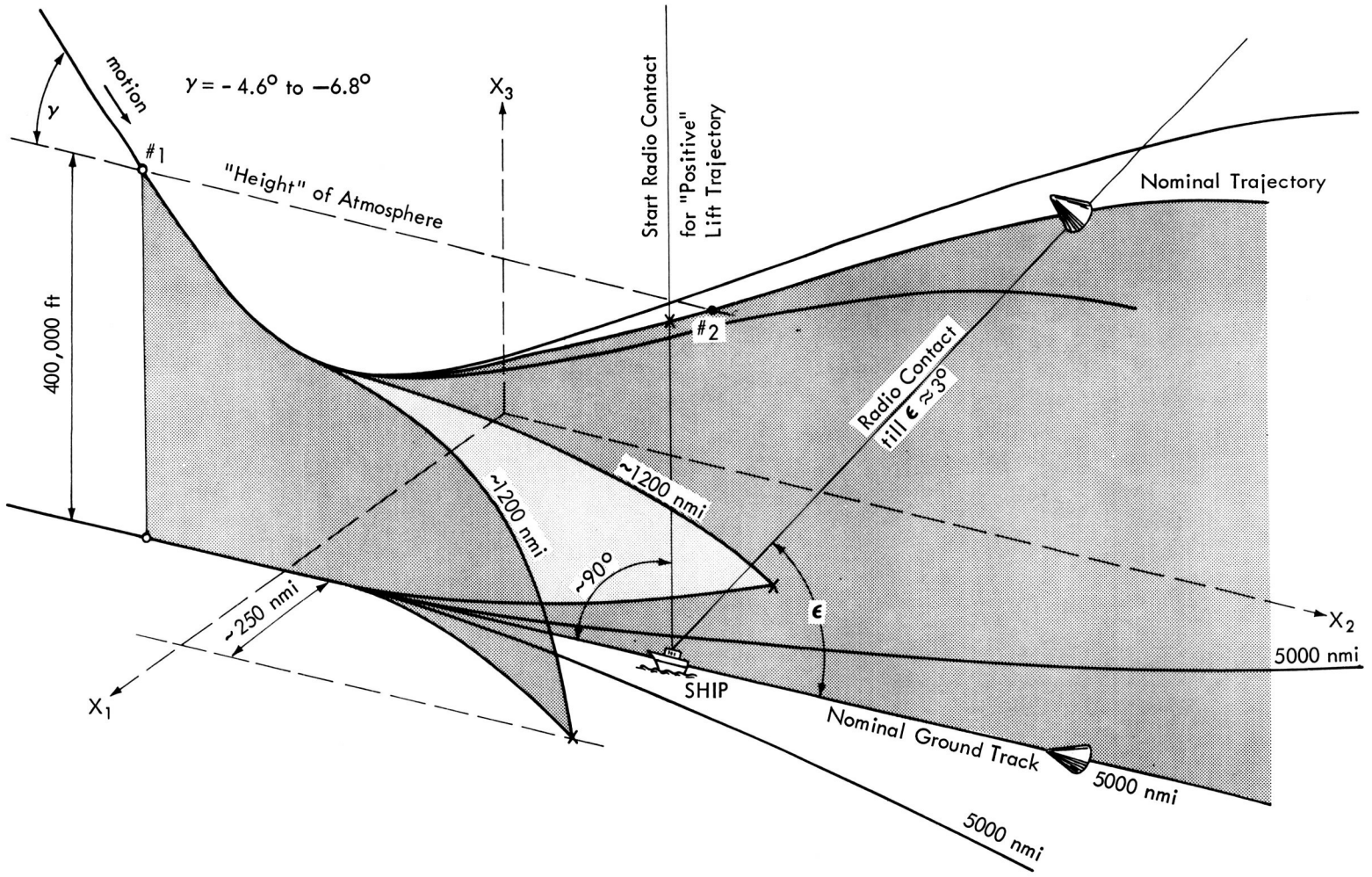

Figure 2 - Re-Entry Trajectories in 3-Dimensions

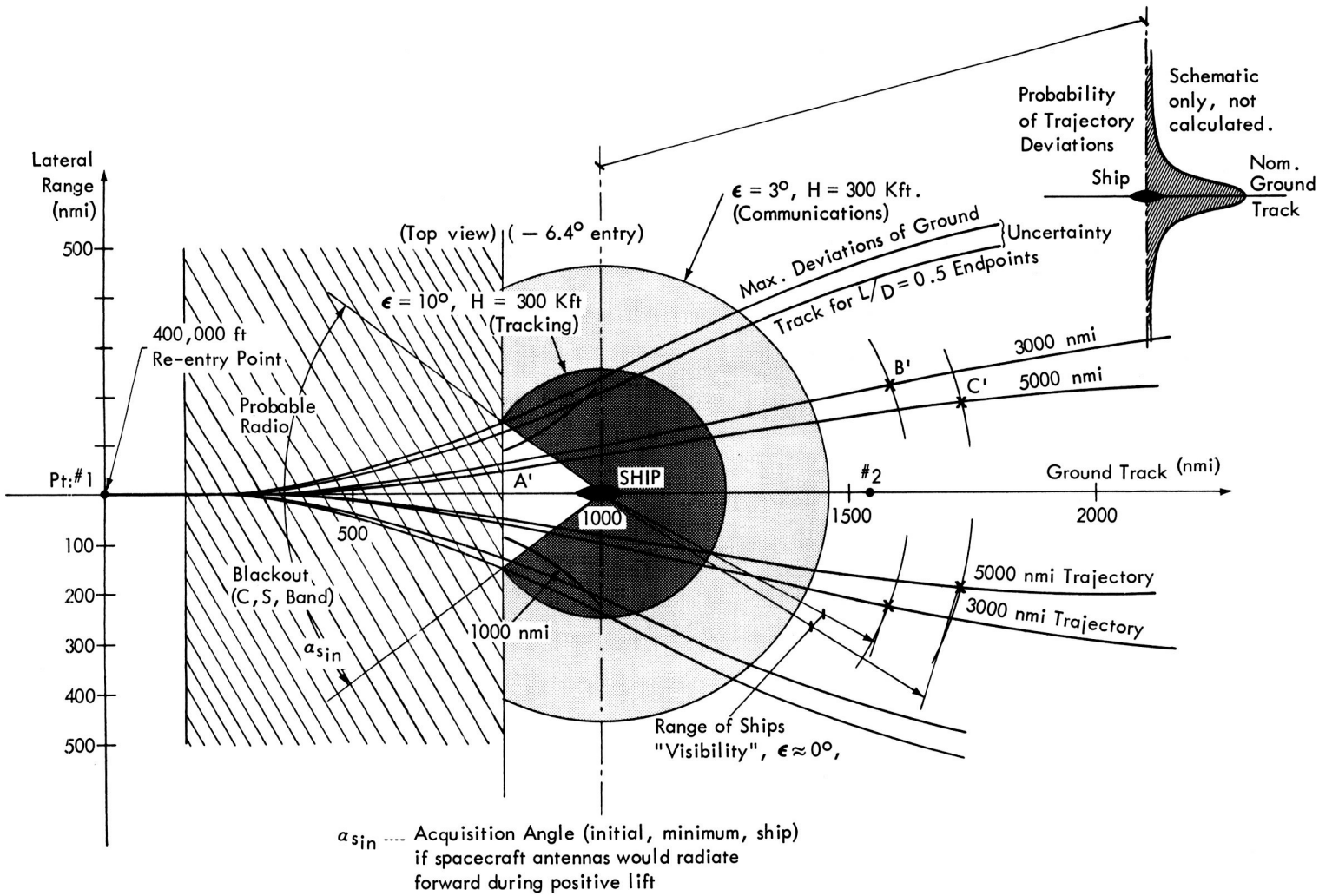

Figure 3 - Apollo Re-Entry Ground Tracks

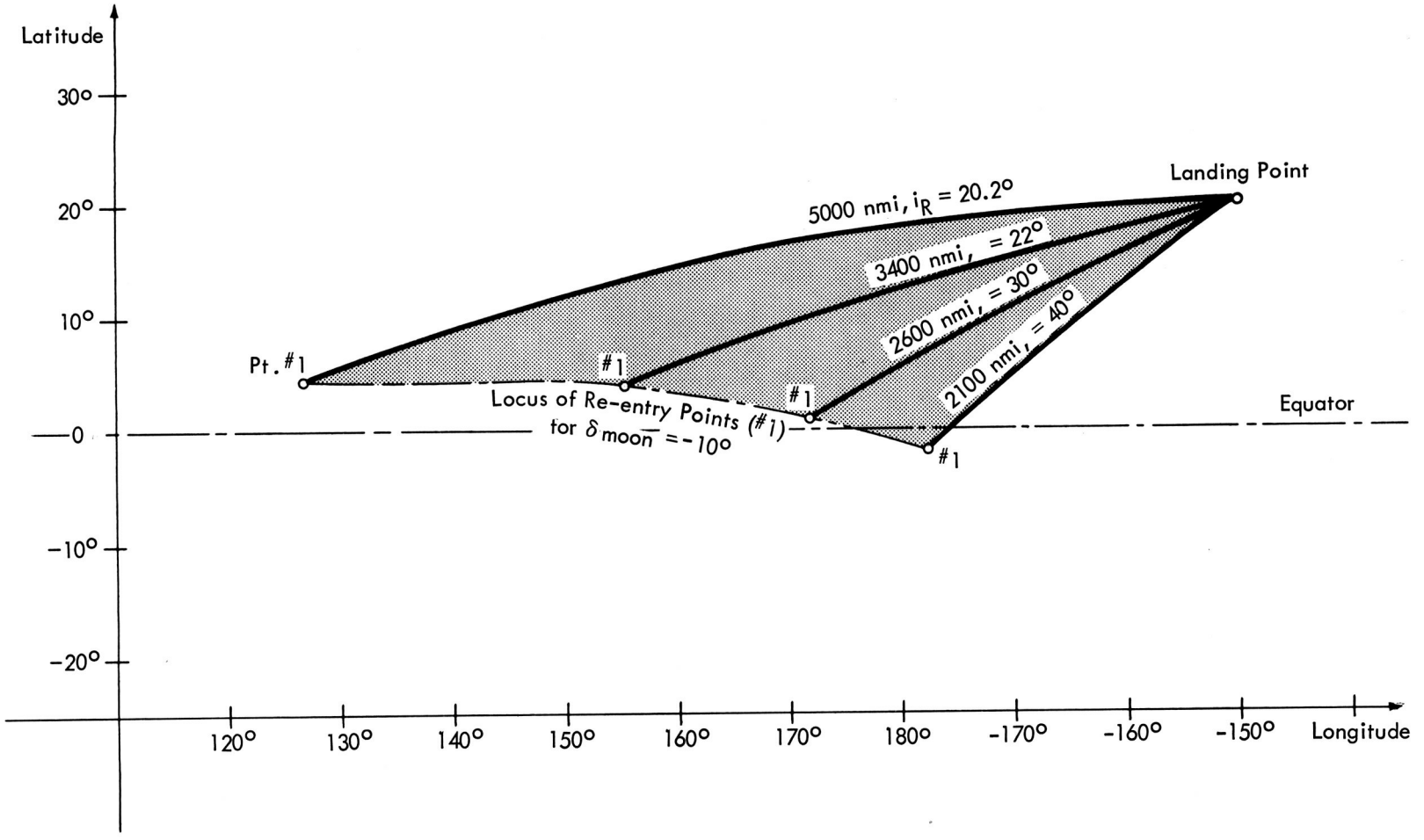

Figure 4 - Re-Entry Ground Tracks for Various Lunar Return Inclinations i_R

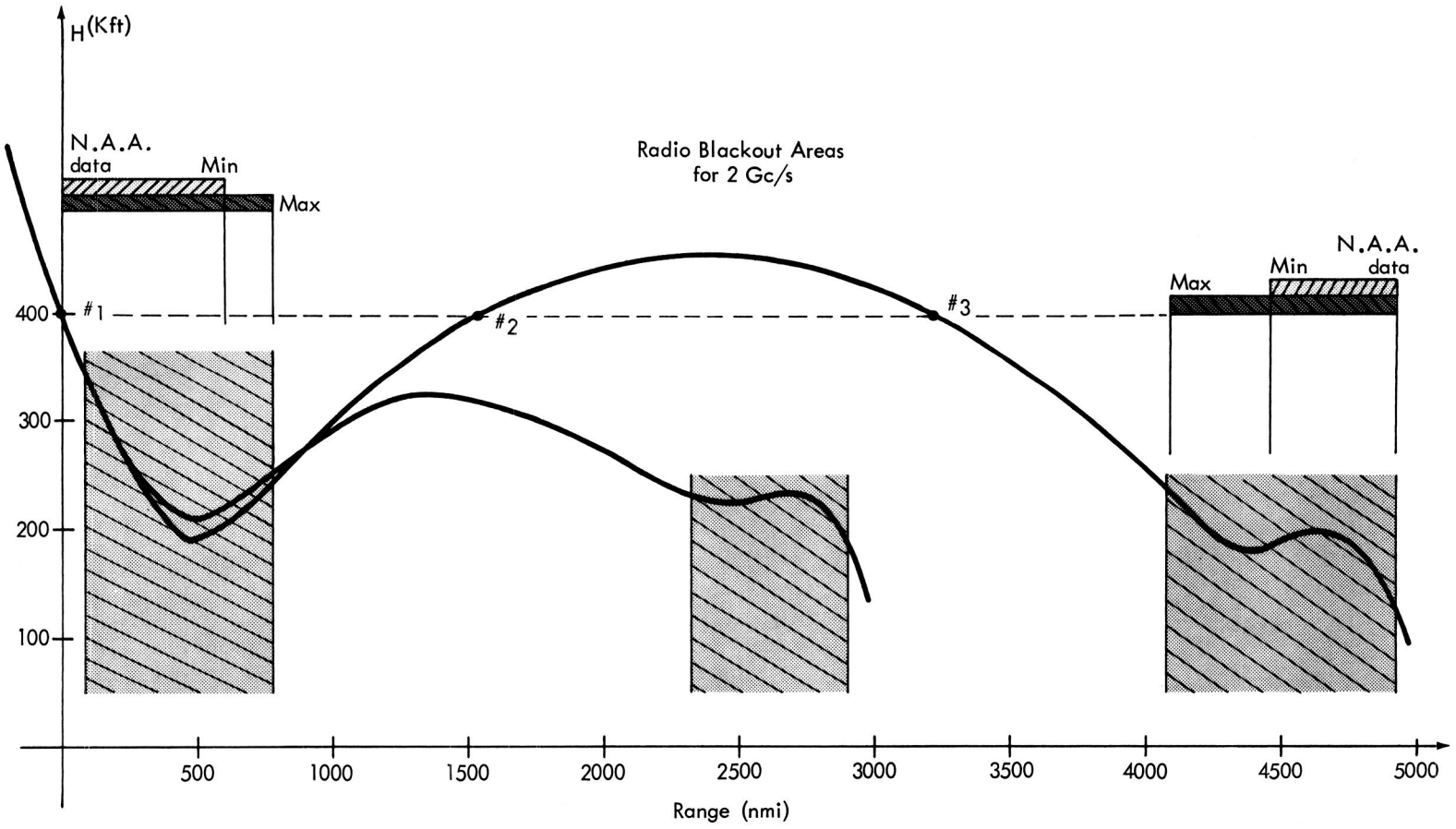

Figure 5 - Apollo Re-Entry Trajectories

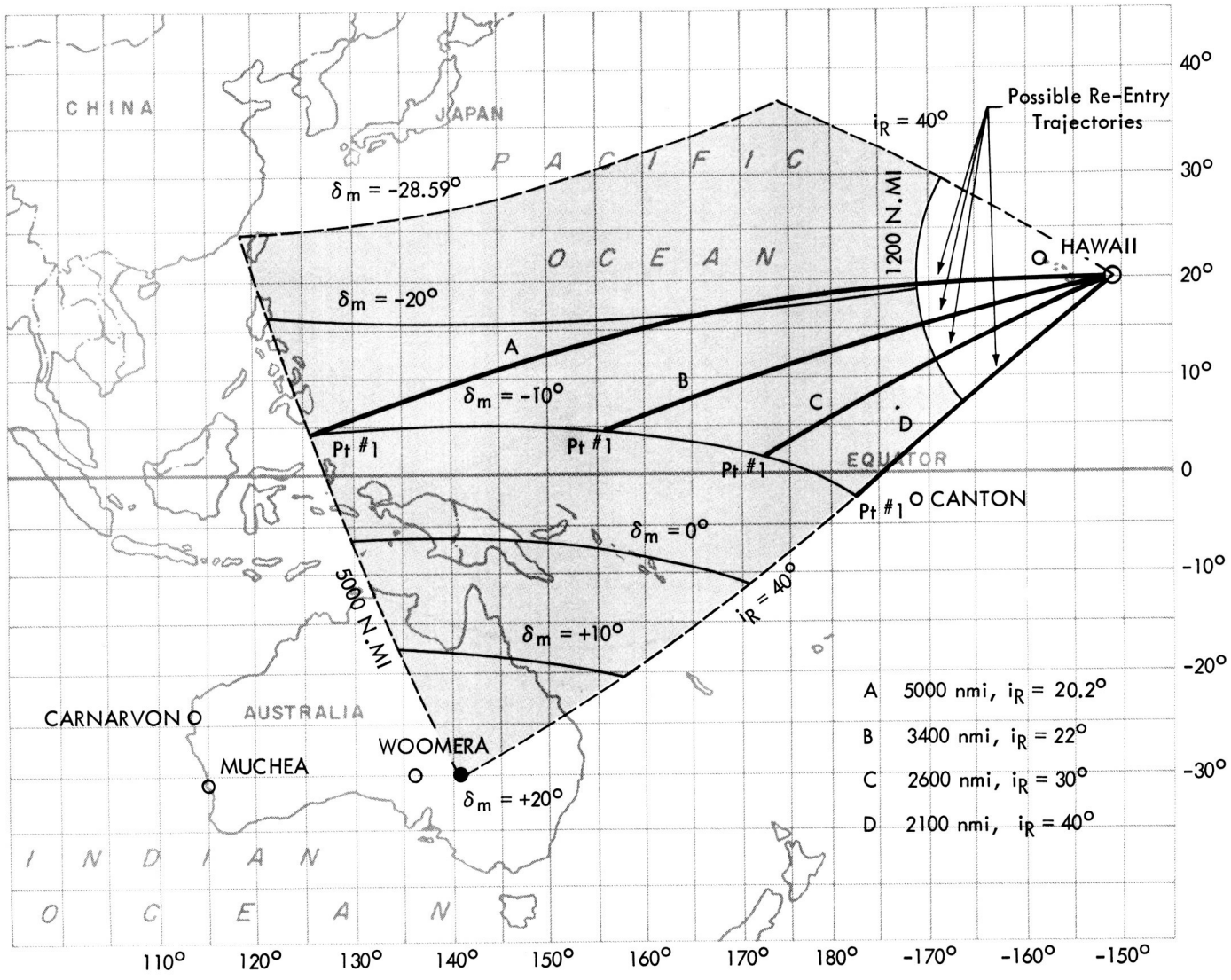

Figure 6 - Locus of Re-Entry Points (Northern Landing Site)

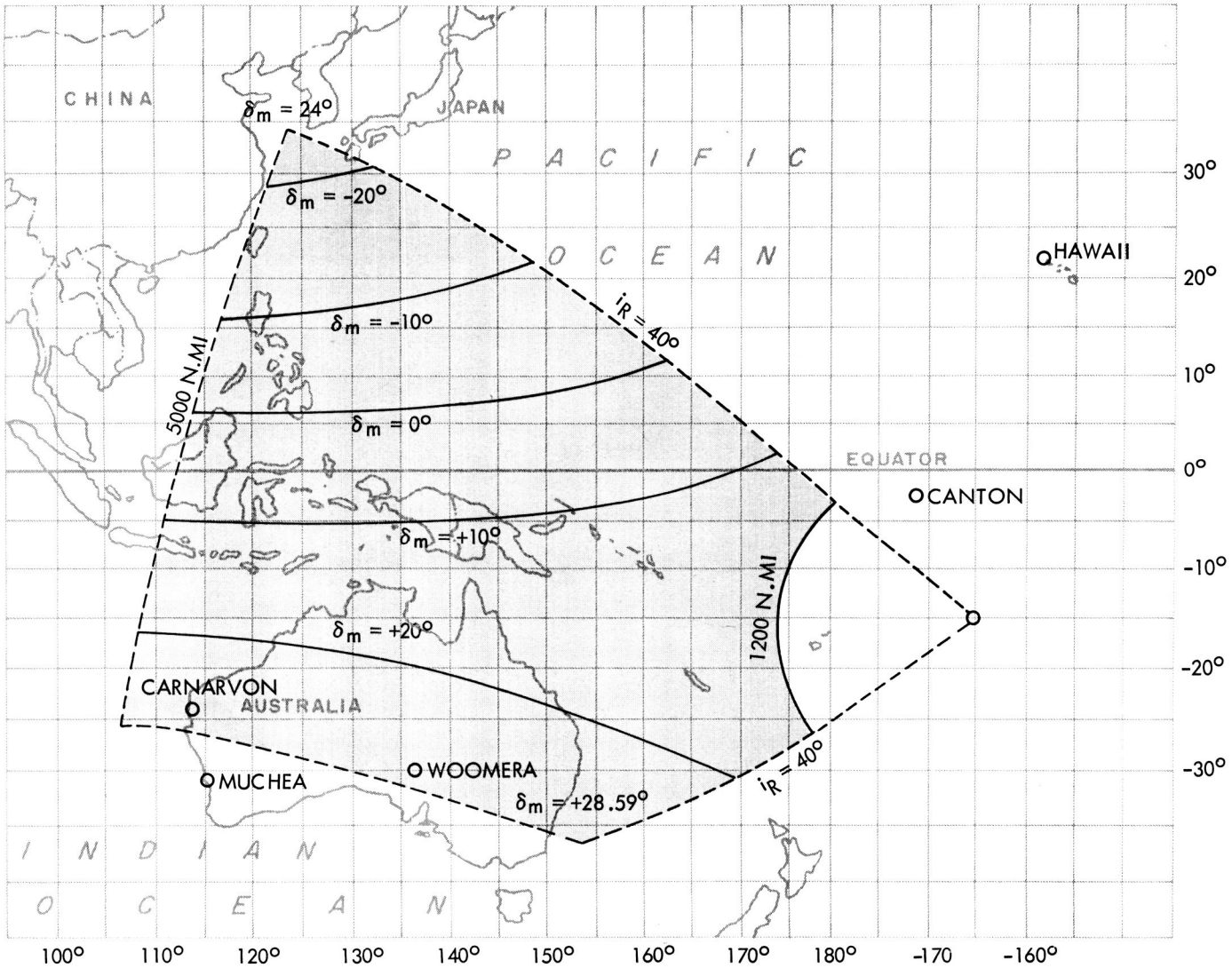

Figure 7 - Locus of Re-Entry Points (Southern Landing Site)

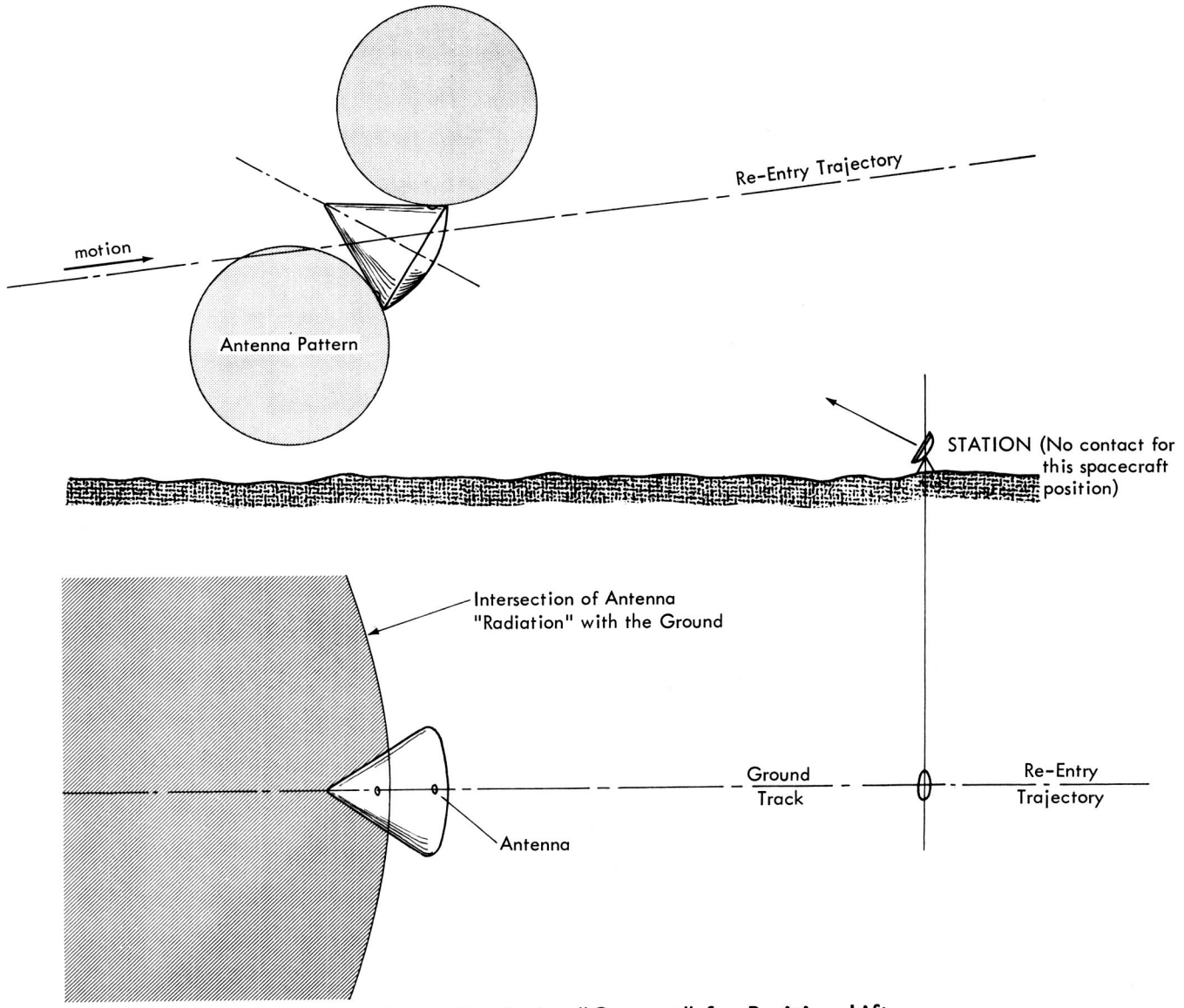

Figure 8 - Radio "Contact" for Positive Lift

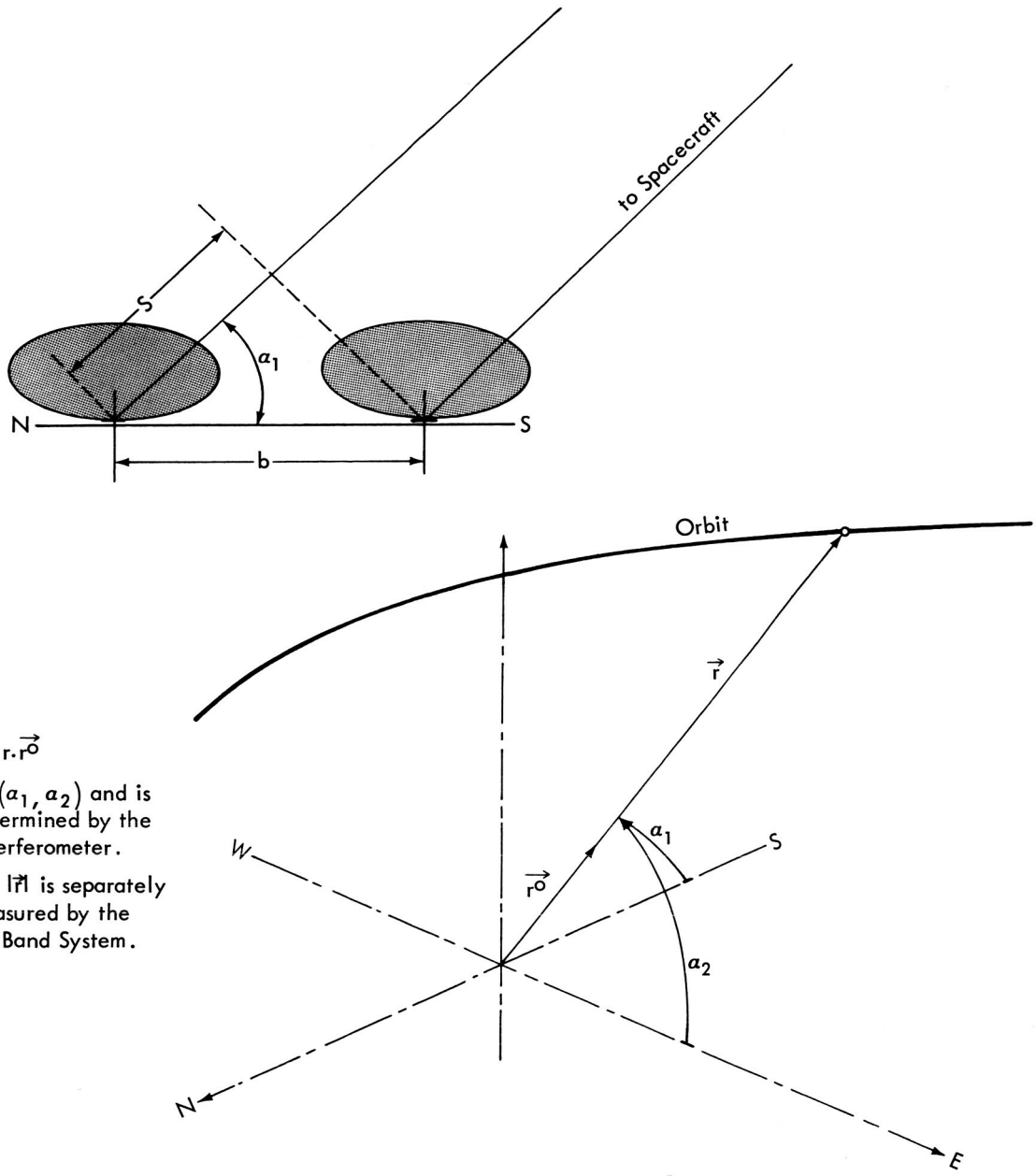

$\vec{r} = r \cdot \vec{r^o}$

$\vec{r^o}$ (α_1, α_2) and is determined by the Interferometer.

$r = |\vec{r}|$ is separately measured by the US Band System.

Figure 9 - Schematic of Re-Entry Interferometer

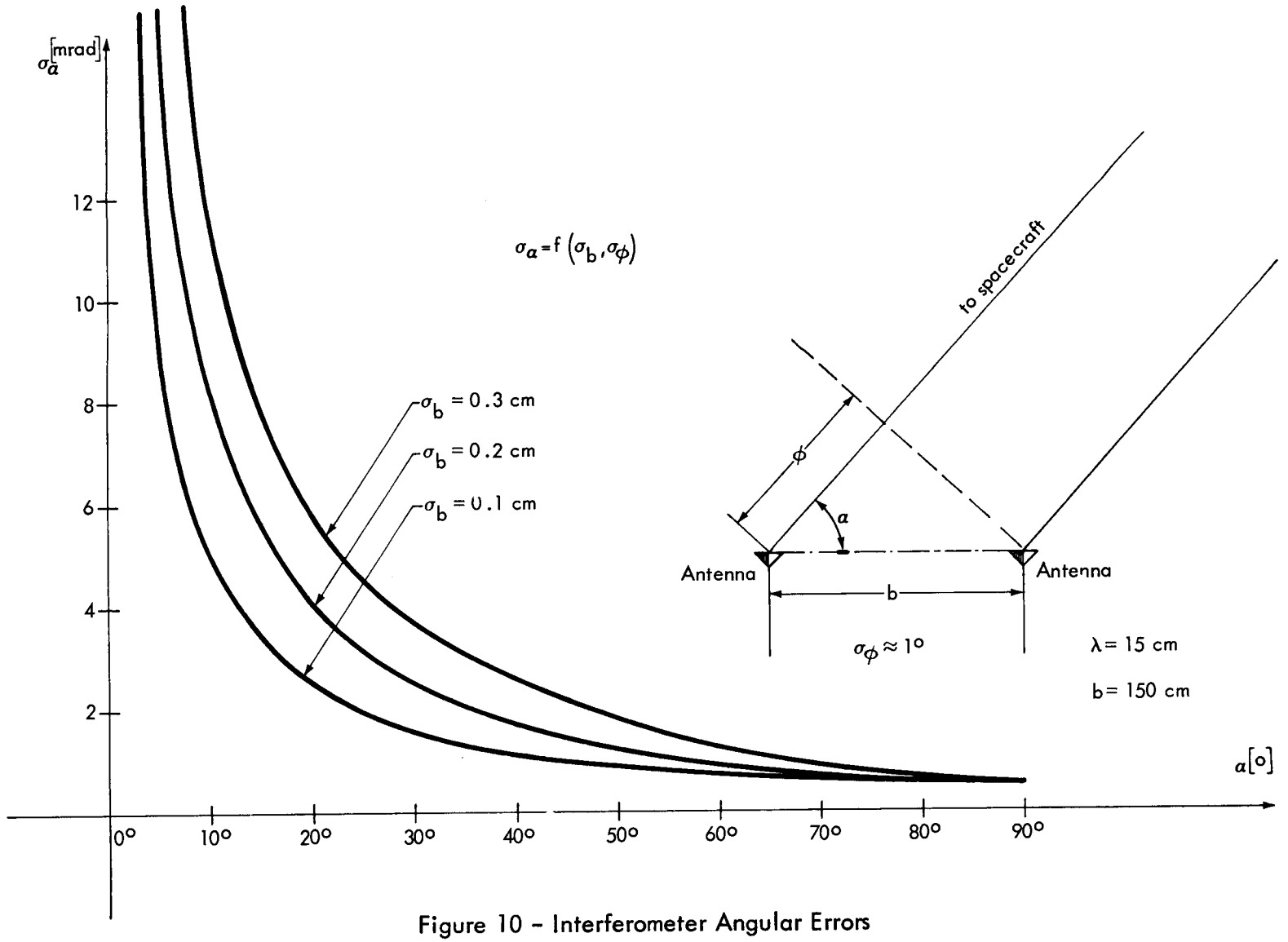

Figure 10 - Interferometer Angular Errors

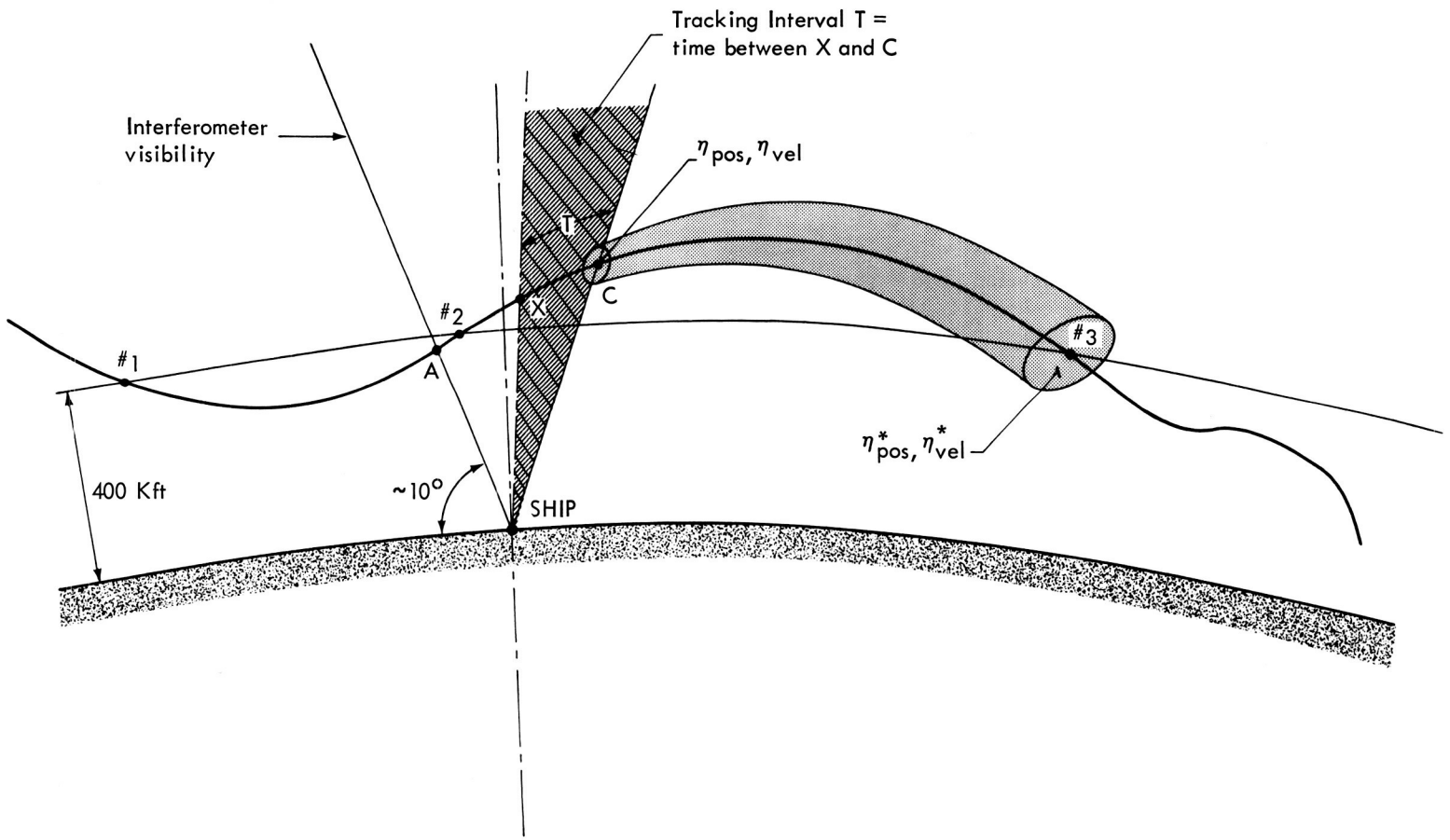

Figure 11 - Schematic of Re-Entry Tracking and Error Projection

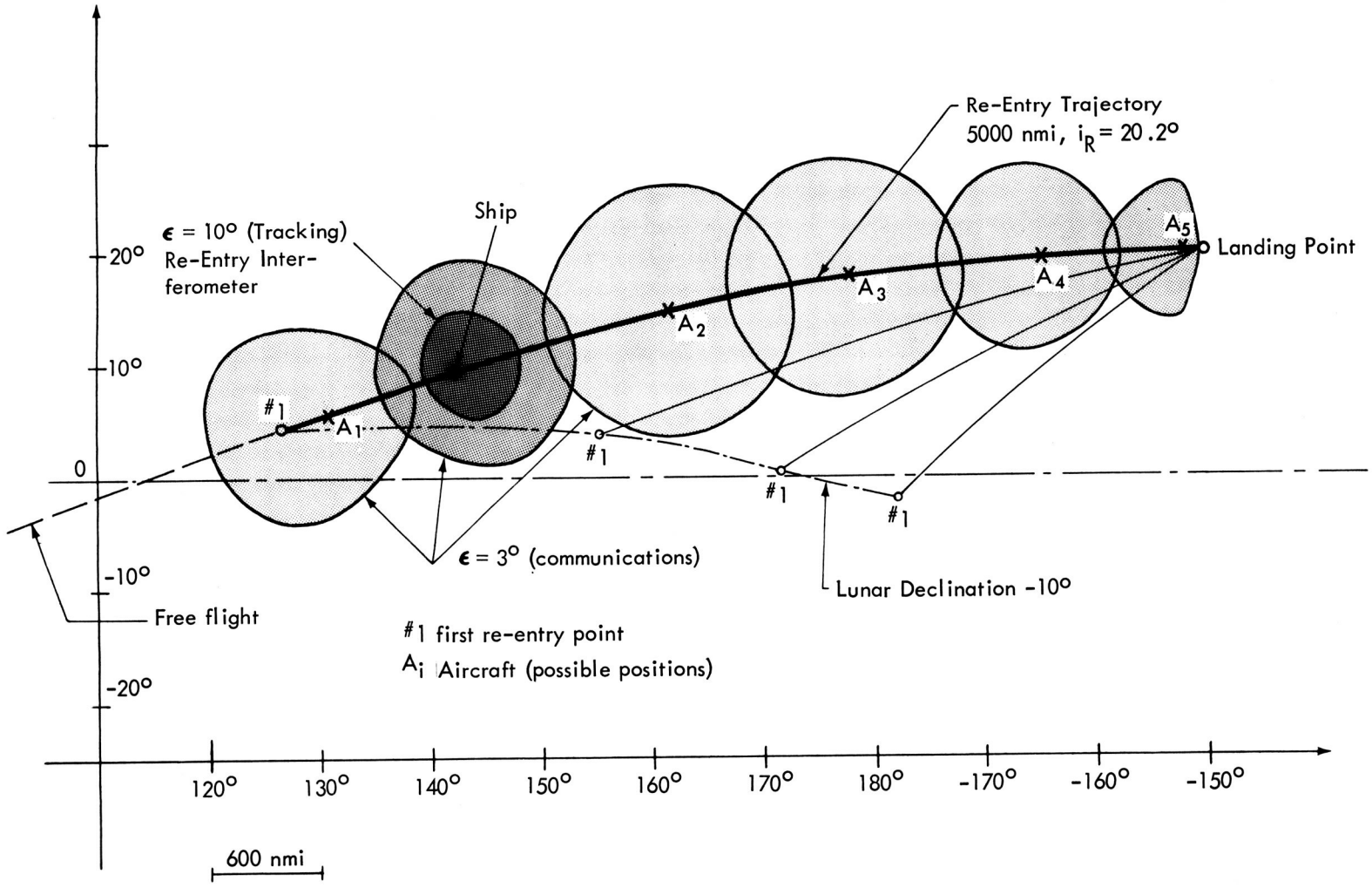

Figure 12 - Apollo Re-Entry Tracking and Communications

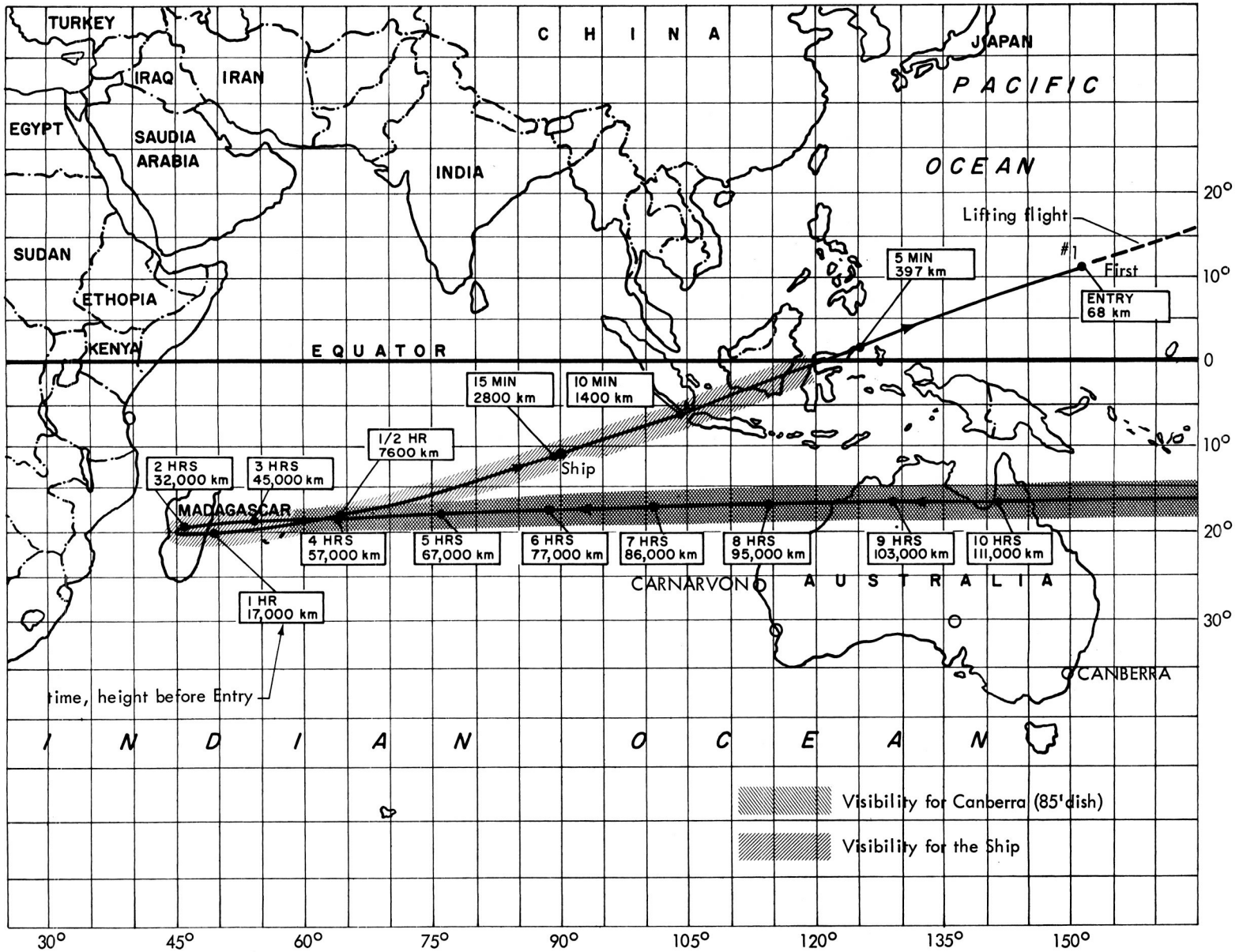

Figure 13 - Example of a Lunar Return Trajectory $i_R = 20.1°$

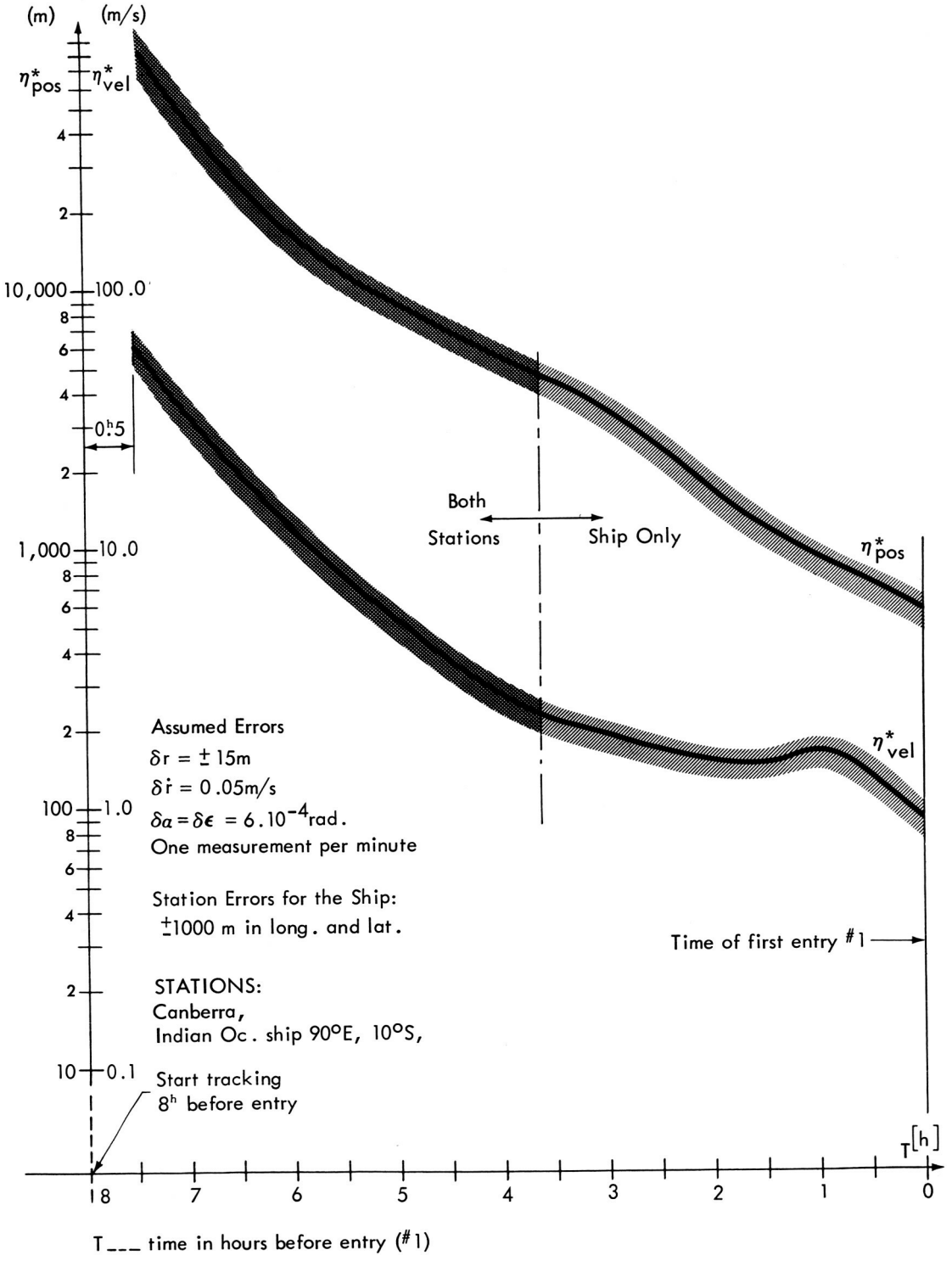

Figure 14 - Position and Velocity Errors Predicted to the Entry Point #1

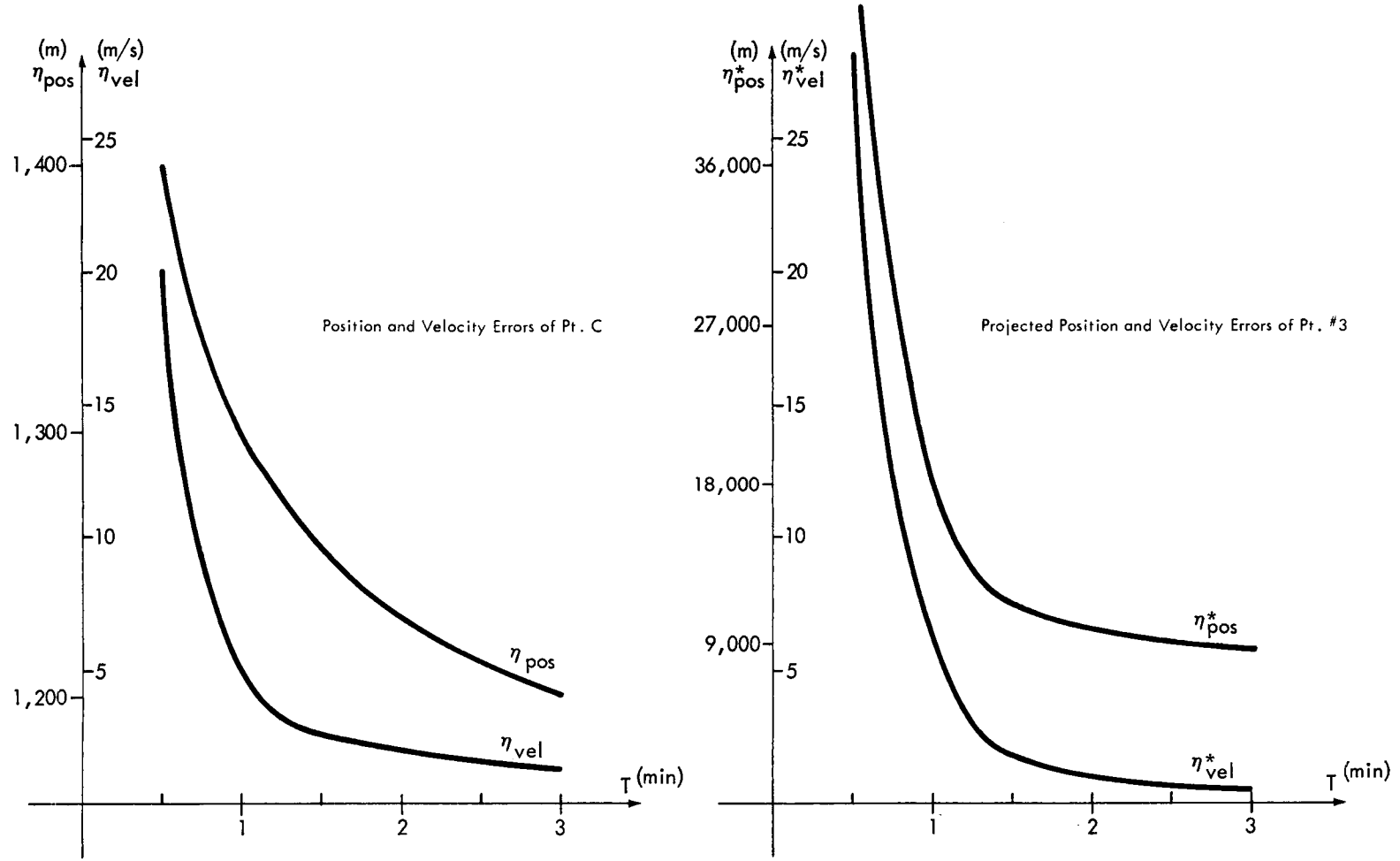

Ships position errors
$\pm$1 km in Lat. and Long.

Figure 15 - Re-Entry Tracking Errors and Their Projections

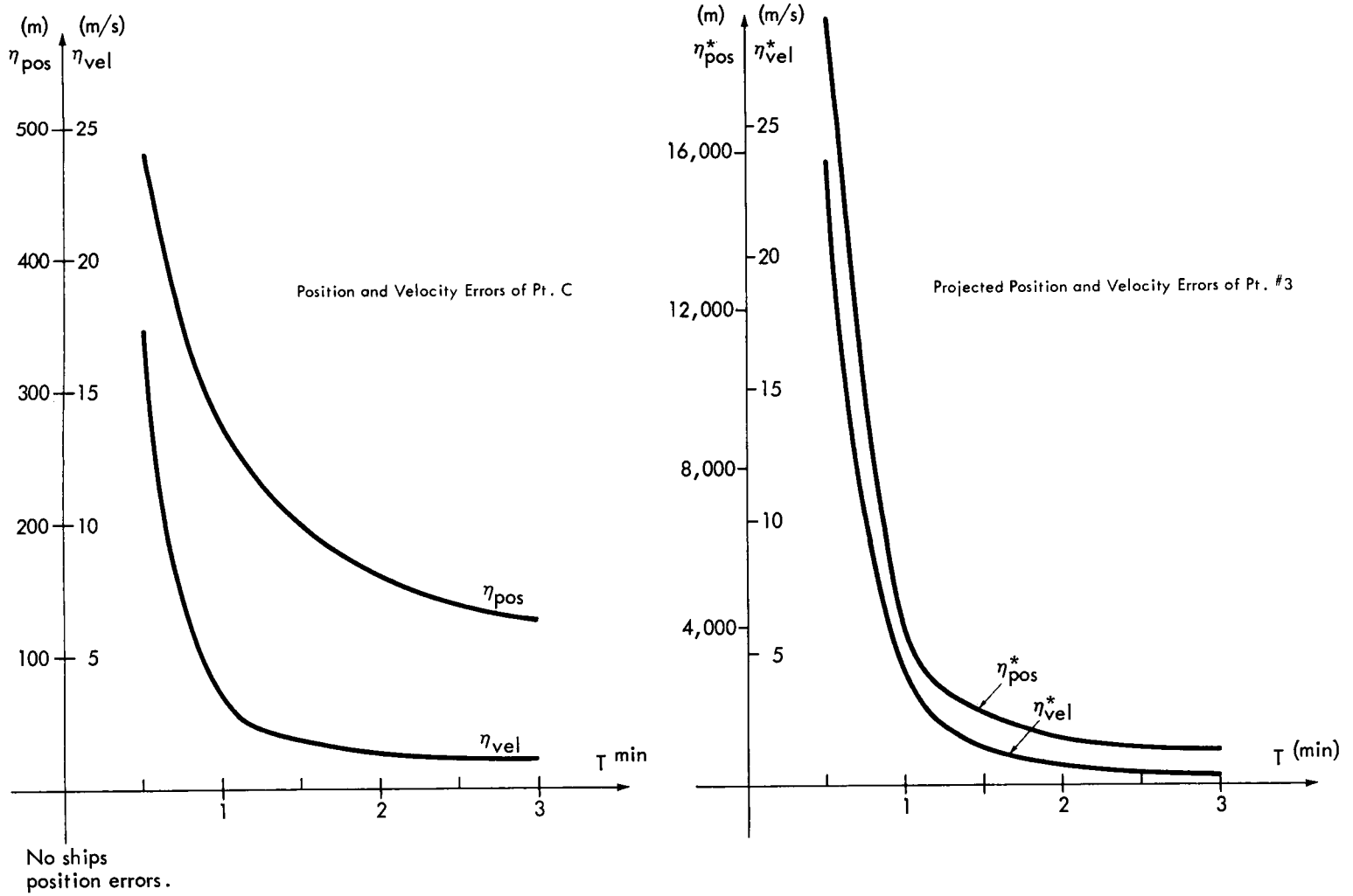

Figure 16 - Re-Entry Tracking Errors and Their Projections

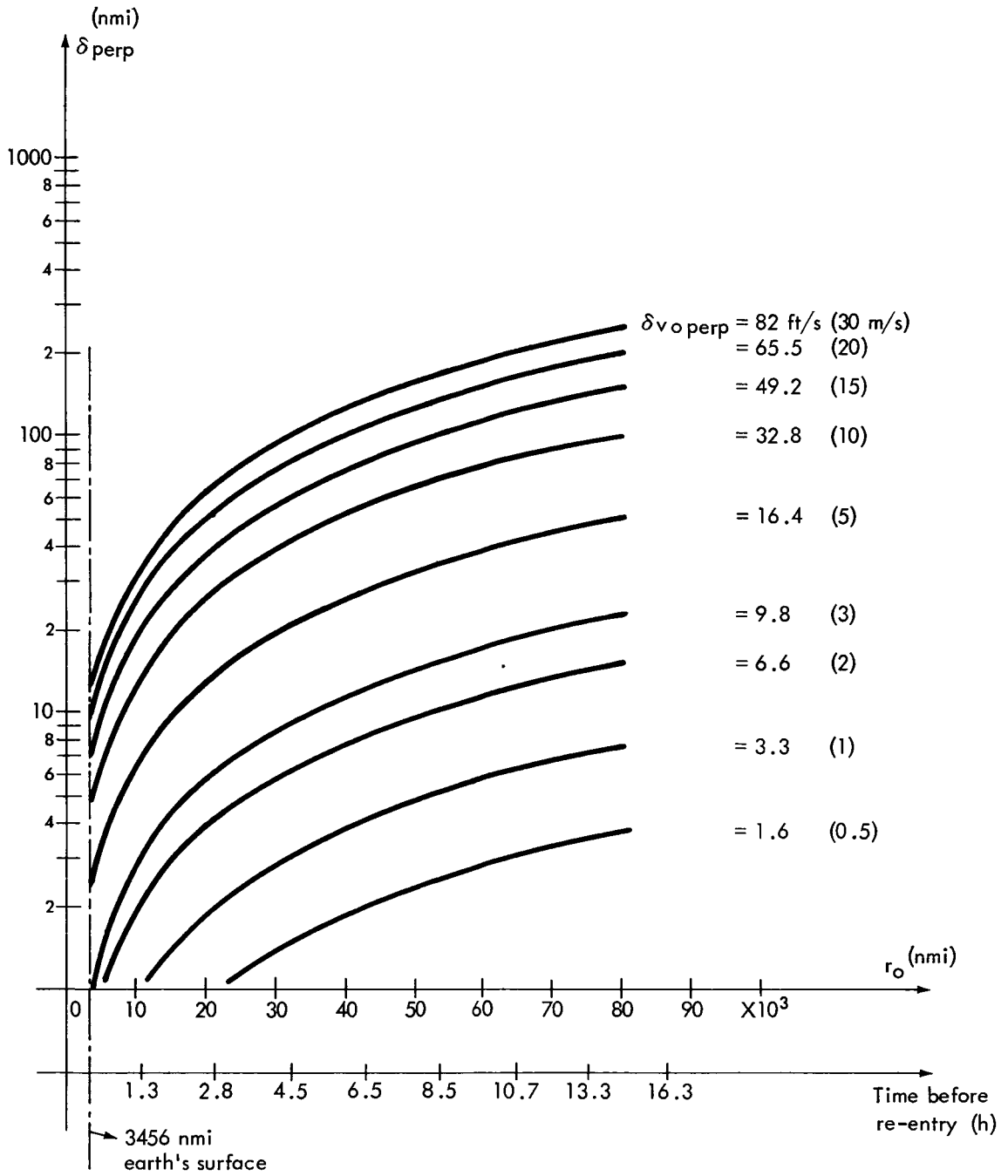

Figure 17 - Variations of the Entry Point Perpendicular to the Track

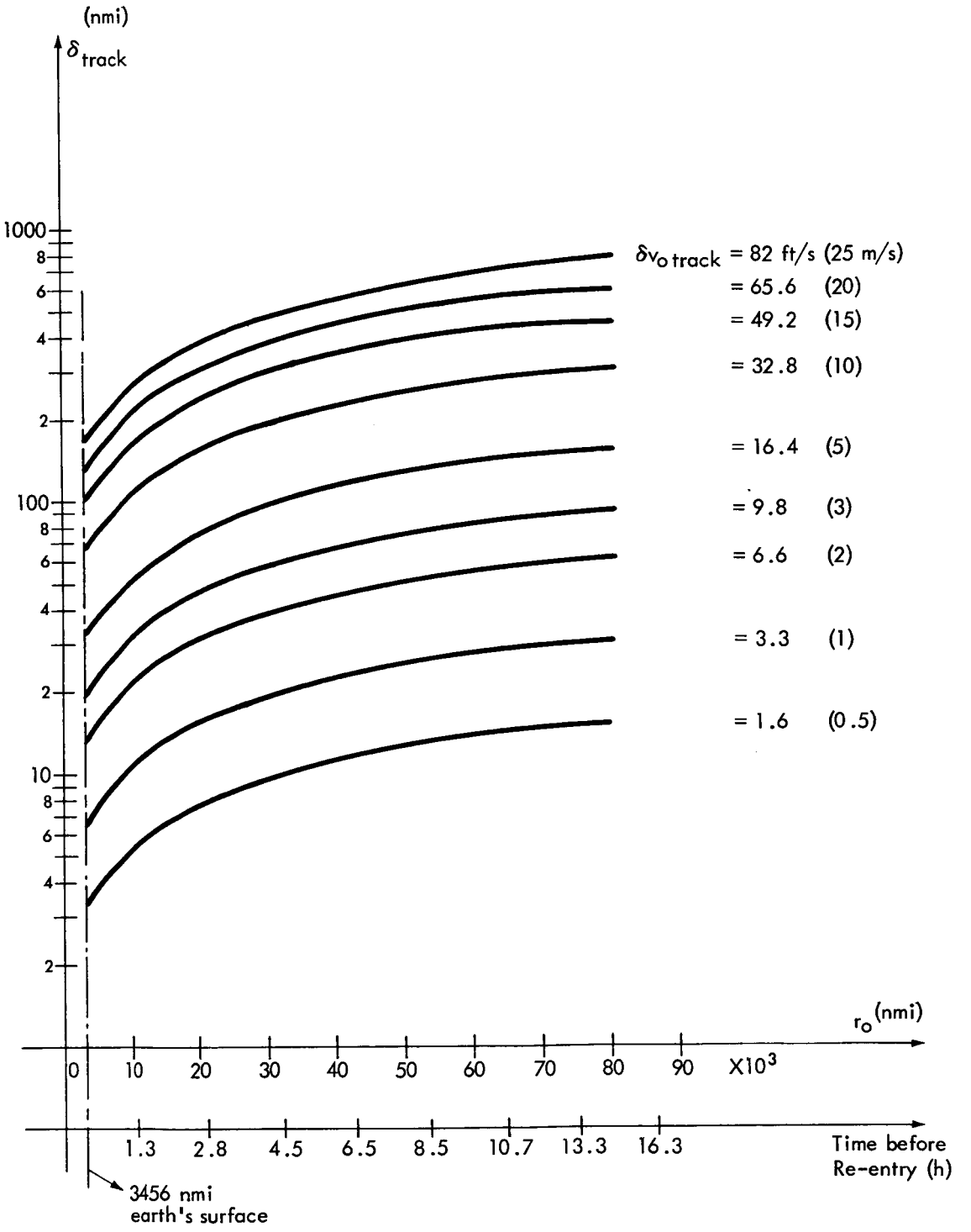

Figure 18 - Variations of the Entry Point Along the Track